Superelastic SMA Belleville washers for seismic resisting applications: experimental study and modelling strategy

Cheng Fang[a)], Xiaoyi Zhou[b)*], Adelaja Israel Osofero[c)], Zhan Shu[a)], Marco Corradi[d)]

[a)] *Department of Structural Engineering, School of Civil Engineering, Tongji University, Shanghai 200092, China*
[b)] *School of Civil Engineering & Geosciences, University of Newcastle, Newcastle upon Tyne, NE1 7RU, UK*
[c)] *School of Engineering, University of Aberdeen, Aberdeen, AB24 3FX, UK*
[d)] *Department of Mechanical & Construction Engineering, Northumbria University, Wynne-Jones Building, Newcastle upon Tyne NE1 8ST, UK*
** Corresponding author: email: xiaoyi.zhou@ncl.ac.uk, Tel: +44 (0) 191 208 7924*

Abstract: This study sheds considerable light on the potential of superelastic Shape Memory Alloy (SMA) Belleville washers for innovative seismic resisting applications. A series of experimental studies were conducted on washers with different stack combinations under varying temperatures and loading scenarios. The washers showed satisfactory self-centring and energy dissipation capacities at room temperature, although slight degradations of the hysteretic responses accompanied by residual deformations were induced. The hysteretic loops became stable after a few number of cycles, indicating good repeatability. The washers also showed good flexibility in terms of load resistance and deformation, which could be easily varied via changes in the stack combination. Compromised self-centring responses were observed at temperatures below 0 °C or above 40 °C, and a numerical study, validated by the experimental results, was adopted to further investigate the deformation mechanism of the washers. A further phenomenological model, taking account of the degradation effects under varied temperatures, was developed to enable effective and accurate simulation of devices incorporating the washers. Good agreements were observed between the test and simulation results, and the model was shown to have good numerical robustness for wide engineering applications.

Keywords: shape memory alloy (SMA); superelastic; Belleville washers; self-centring; numerical study; phenomenological model.

1. Introduction

Shape Memory Alloys (SMAs), as a class of smart materials, have been successfully employed in the aerospace (e.g. aircraft wings and smart helicopter blades) and medical (e.g. arterial stents and catheters) industries [1-2]. SMA has two unique properties, namely, Superelastic Effect (SE) and Shape Memory Effect (SME) [3]. When SMA is deformed above the austenitic finish temperature A_f, it starts to accommodate the strain by transforming from the austenitic phase into the detwinned martensite phase. However, the deformation (up to 8-10% strain) can be recovered spontaneously after unloading, i.e. the detwinned martensite will revert back to austenite. This phenomenon is known as the Superelastic Effect (SE). On the other hand, when the SMA is deformed below the martensitic finish temperature M_f, it is transformed from the twinned martensitic phase to the detwinned martensitic phase. Upon unloading, residual deformation remains, but heating the deformed SMA can

promote strain recovery. This phenomenon is known as Shape Memory Effect (SME). With continuous improvement in metallurgic technology and reduction in manufacturing cost, along with better understanding of the material property, the practical applications of SMA are nowadays stretching beyond the existing high-value fields, where one of the new areas of application is civil engineering. Special interest is given to self-centring seismic control, where SE of SMA is widely utilized in passive control, while SME is normally considered in active control or semi-active control [4]. Although both passive and active (semi-active) controls can be promising strategies against seismic hazard, more attention has been paid to SE of SMA due to the inherent characteristics such as spontaneous self-centring, hysteretic damping, and free of external power source.

Innovative devices and applications based on superelastic SMA have been explored by a large number of researchers. As wire is one of the most convenient forms of SMA due to its ease of manufacture and high utilisation efficiency, significant research efforts have been devoted to the application of SMA wires in base isolators [5-6], dampers [7-8], and bracing systems [9-11]. While good self-centring abilities coupled with reasonable energy dissipation were generally observed in these devices or structural components, a large number of wires need to be included to ensure that the levels of load resisting capacity match the magnitude required for accommodating 'structural-level' loading. This can complicate the arrangement of the wires and more importantly, complicate the gripping (end-fixing) strategy due to the difficulty of effective gripping over the smooth wire surface. As most of the existing research on SMA wire-based devices were either proof-of-concept (e.g. numerical and theoretical) or small-scale tests (where small diameter SMA wires were adopted), the efficiency of SMA wires for large-scale structural components/facilities should be further examined. Using stranded SMA ropes instead of smooth SMA wires may be an encouraging solution. Recent studies [12-13] showed that the performance of stranded SMA ropes was dependent on the helix angle, and the energy dissipation capacity and self-centring ability were less satisfactory than single SMA wires. Moreover, the available studies mainly focused on the uniaxial cyclic performance of the strands with no specific discussion on the gripping strategy. Larger diameter SMA bars can be another alternative to SMA wires in order to achieve a reasonable level of load resistance for structures. The ends of the SMA bars are often threaded such that they can be used as bolts for connections [14-17] and bridge restraining devices [18]. However, relevant test programmes [15-16] showed that SMA bolts were quite susceptible to fracture over the threaded area. Increasing the net threaded-to-shank area ratio (which decreases the stress demand over the threaded area) may improve the ductility of the SMA bolts.

To potentially address the above mentioned barriers to the use of SMA, a new form of SMA component, namely, superelastic SMA Belleville washer, could be an important addition to the 'arsenals' against seismic hazard. A Belleville washer [19], also known as conical spring washer or

disc spring, is a mechanical component which can sustain a wide range of loads with small installation space. Because of their annular shape, as shown in Fig. 1, force transmission is relatively even and concentric and thus they can be more stable compared with other springs, e.g. helical springs. When Belleville washers are endowed with superelastic ability, which enables self-recovery and hysteretic damping, their application may be further expanded. Early studies on SMA Belleville washers were mainly for electrical applications with the main purpose of electric circuit stabilisation [20]. The potential of superelastic SMA Belleville washers as seismic resisting dampers was first investigated by Speicher et al. [21]. The washers showed satisfactory self-centring ability, but the hysteretic stabilisation properties with repeated cycles was not revealed as only a limited number of cycles were performed. It was also found that the load carrying capacity decreased significantly with increase in deformation beyond the peak load, and the resulting 'invert' tendency compromised the damping performance of the washer groups. It was argued that the snap-through behaviour was due to the relatively high cone angle θ (Fig. 1) considered for the test washers. A later numerical investigation [22] considered different geometric shapes of the washers, and the results showed that good self-centring and energy dissipation responses could be achieved if the geometric configuration of the washers is appropriately designed. More recently, Maletta et al. [23] introduced a new thermomechanical process for producing SMA Belleville washers through disk cutting and a successive shape setting by heat treatment. This was then followed by Finite Element (FE) studies on the influences of washer geometric configuration and temperature on their cyclic performance, but no further experimental proof was provided. A semi-analytical model, which was found to correlate well with the FE predictions, was also developed [24]. Other types of SMA components, e.g. SMA rings [25-26], are also under development.

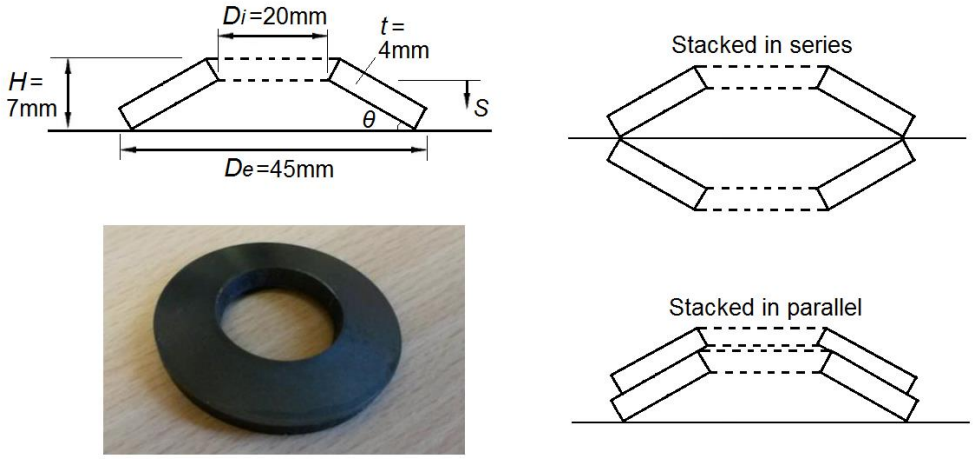

Fig. 1 SMA Belleville washers and key dimensions (not-to-scale)

It can be seen from the above discussion that the research on SMA Belleville washers for seismic engineering is quite promising but is still in its early stage, and in particular, their cyclic

repeatability and temperature dependence have not been physically investigated. Information on effective modelling of SMA Belleville washers is also insufficient. The present work, done in collaboration with MEMRY (SMA manufacturer), discusses the mechanical property and modelling strategy of superelastic SMA Belleville washers for innovative seismic resisting applications. The study will reveal the feasibility of commercializing SMA for the construction industry, and this will benefit communities of both civil engineers and material scientists.

2. Experimental programme

2.1 *Test specimens*

A total of 11 specimens, including ten NiTi SMA-based washer specimens and one commercial stainless steel washer, were tested in this experimental programme. The main test parameters were temperature and arrangement of washers. The influence of maximum deformation (S_{max}) on the mechanical properties of the washers was also studied. The basic test parameters are given in Table 1. The same geometric configuration was chosen for all the SMA Belleville washers: the external diameter (D_e) and internal diameter (D_i) were 45 mm and 20 mm, respectively; the overall height (H) of the washer was 7 mm, and the thickness (t) was 4mm. The considered geometric configuration led to a cone angle (θ) of 13.5°. The key dimensions are illustrated in Fig. 1. The SMA Belleville washers were produced by the material supplier MEMRY (www.memry.com). Per information from the supplier, the austenite finish temperature A_f was 4.5 °C such that the washers can exhibit superelastic behaviour at ambient temperatures (i.e. room temperature was approximately 23 °C for the current test). The composition of all the specimens was nearly identical, with 55.87% nickel – 44.13% titanium by weight. All the specimens were hot-rolled with an appropriate heat treatment by the material supplier, and they were tested in received condition with no further heat treatments. The stainless steel washer was purchased from a commercial washer supplier, and the dimension was slightly different to the SMA Belleville washers: D_e = 50 mm, D_i = 22 mm, t = 5 mm, and the allowable deformation = 1 mm. The stainless steel washer test was a demonstration test for comparison purpose only. All the specimens were virgin without pre-training before the tests.

Table 1 Test parameters

Specimen code	S_{max} (mm)	Temperature (°C)	Arrangement
SMA1-a	2.7	23	Single
SMA1-b	2.7	23	Single
SMA1-H	1.3	23	Single
SMA2-S	5.4	23	Two in series
SMA2-P	2.7	23	Two in parallel
SMA1-T(10)	2.7	10	Single
SMA1-T(40)	2.7	40	Single
SMA1-T(60)	2.7	60	Single
SMA1-T(0~23)	2.7	0~23	Single
SMA1-T(-20~23)	2.7	-20~23	Single

SS1	1.0	23	Single

The specimens were tested isothermally under various temperatures ranging from -20 °C to 60 °C. Single (individual) washer tests were conducted, and in addition, washer groups consisting of two washers stacked in two different ways, i.e. in series and in parallel (as illustrated in Fig. 1), were also investigated. For easy identification, each specimen was assigned with a specimen code according to its washer arrangement, temperature, and loading condition. The specimen code starts with the material type, i.e. SMA or SS (stainless steel), followed by 1 or 2 indicating the number of washers in the test specimen, and ends with a description of the test, where 'a' and 'b' means two duplicate tests on single washer; 'H' means only half of S_{max} was applied; 'S' and 'P' indicate two washers stacked in series and in parallel, respectively, and 'T' indicates that the test was conducted under a temperature (which is shown after 'T') different from the room temperature (23 °C). It should be noted that for some specimens, e.g. specimen SMA1-T(-20~23), two temperatures were included in the specimen code, this is because the test was first conducted under a temperature below A_f and then the temperature was increased beyond A_f (back to room temperature) for further testing. Details of the test procedures are discussed in the following section.

2.2 *Test setup, procedures, and instrumentations*

The specimens were subjected to compressive cyclic load with a loading frequency of 0.02 Hz under displacement control. The standard maximum displacement S_{max} of each cycle was 2.7 mm, such that the washer could be deformed to an almost flattened state at S_{max}. For specimen SMA1-H, S_{max} = 1.3 mm was considered in order to examine the performance of the washer when only a half of the allowable deformation is utilized. For specimen SMA2-S, where two washers were stacked in series, the maximum displacement was doubled (i.e. 5.4 mm). A single stainless steel washer was also tested and the arrangement of this test was basically the same but with 1 mm maximum deformation. For the specimen tested under the temperature above A_f, the loading-unloading process was repeated for 50 cycles to monitor the degradation response of the hysteretic curve. For those tested below A_f, where the superplastic behaviour could not be fully developed, 10 cycles were carried out first, and then the temperature was increased and additional 50 loading cycles were performed at room temperature. These stepped-temperature tests were used to investigate the influence of low temperature weather conditions as well as the ability of the washers to regain superplastic behaviour with reheating. Before each test (or test stage), the specimen was placed under the required temperature for at least 30 minutes to ensure an even distribution of the internal temperature within the washer.

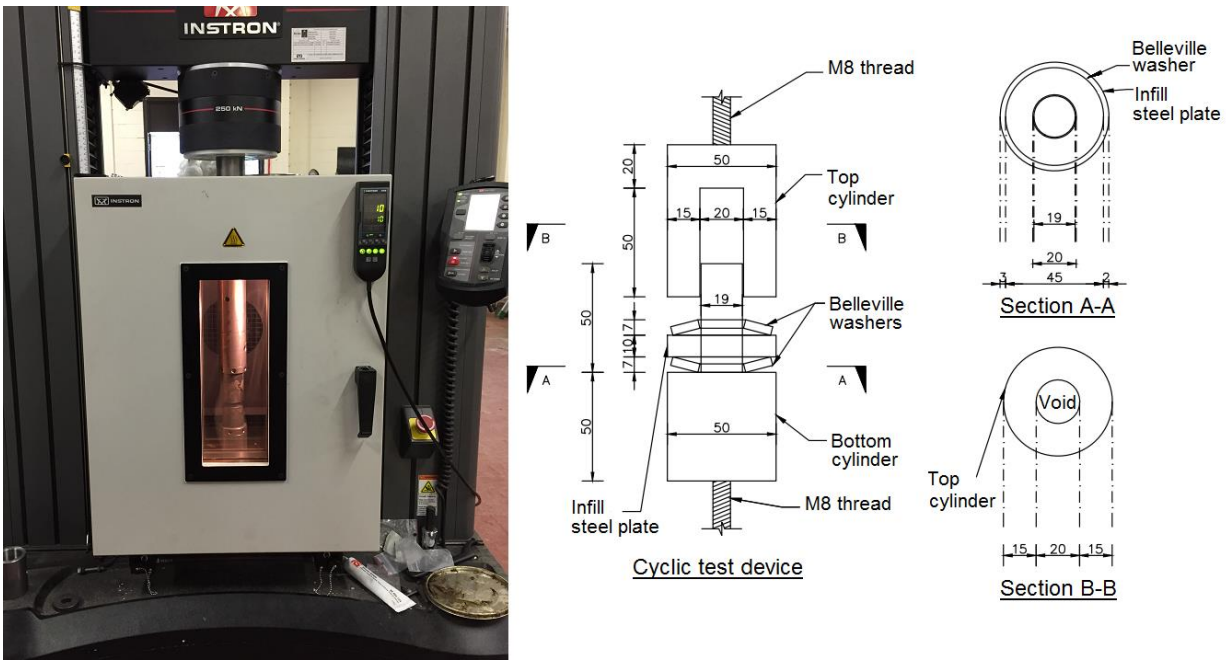

Fig. 2 Photo and details of test setup

The cyclic tests were performed using an INSTRON 5585H Universal Test Machine (UTM) with a maximum loading capacity of 250 kN. The aforementioned loading protocol was implemented and the experimental data (load and displacement) were automatically recorded via built-in load cell and displacement controllers. For the specimens exposed to temperatures other than the room temperature, an environmental chamber was employed which is capable of offering a constant temperature ranging between -70 °C and 350 °C. A bespoke testing device, as shown in Fig. 2, was designed for holding the washers in position throughout the experiment. The device consisted of two cylinders, with the top cylinder fixed to the loading head of the UTM and the bottom one fixed to the base of the machine. The washers were passed through a rod fixed at the surface of the bottom cylinder, and correspondingly a hole was made in the top cylinder to accommodate the rod during the test. By using this piston-type device, the compressive load can be applied uniformly onto the washers and the conditions (e.g. deformed shape) of the washers can be clearly observed during the test. For specimen SMA2-S, where two washers were stacked in series, an additional steel plate was placed between the two washers. Detailed dimensions of the testing device are shown in Fig. 2.

3. Test results and discussions

3.1 *Load-deformation response*

The load-deformation curves of all the specimens are shown in Fig. 3. For the SMA Belleville washers tested under temperatures above A_f (4.5 °C), flag shape hysteretic curves with recognizable forward and reverse transformation plateaus are typically exhibited. The load (of single washer) at maximum deformation ranged between 10 kN and 17.5 kN, and the value tended to increase with increasing temperature. This is due to the well-known austenite and martensite slopes (of phase

diagrams) where the forward/reverse transformation plateaus increase almost linearly with increasing temperature [3], as illustrated in Fig. 4. Considering the maximum compressive deformation of 2.7 mm, the secant stiffness of single washers varied approximately between 3.7 kN/mm and 6.5 kN/mm. Degradations of the hysteretic responses, accompanied by residual deformations, were induced, especially in the first few cycles; however, the hysteretic loops then became stable with increasing number of cycles. The degradation response was mainly due to the Transformation Induced Fatigue (TIF) in SMA, where the significance of TIF depends on various factors, including fabrication process, heat treatment, temperature, loading conditions, etc. [3].

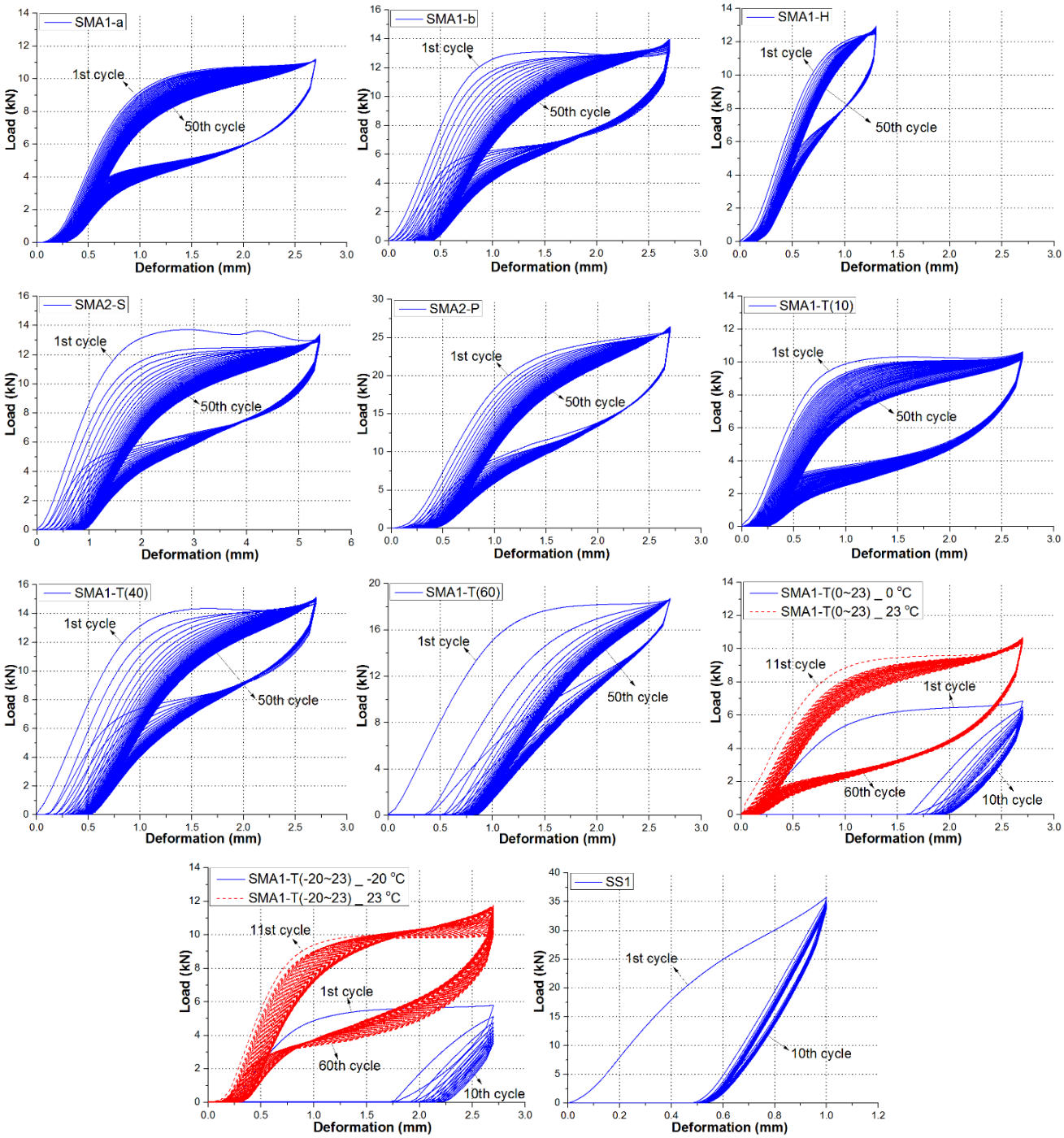

Fig. 3 Load-deformation response of test specimens

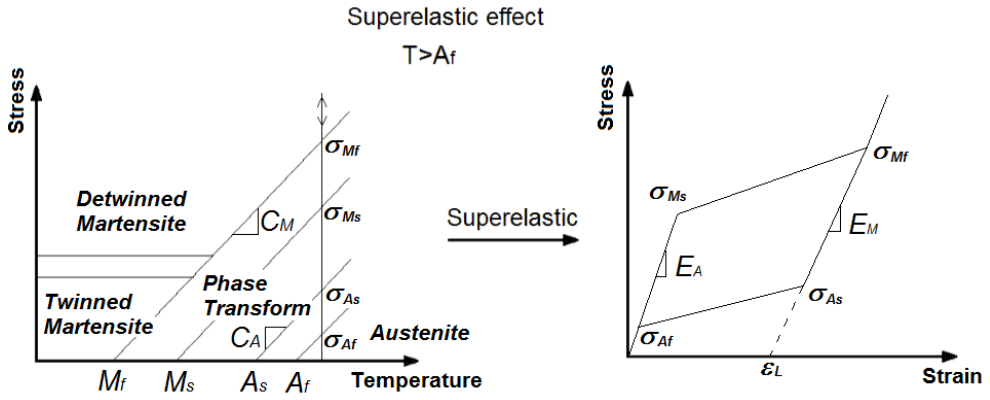

Fig. 4 Phase diagram of superelastic SMA

Very minor 'snap-through' type load-deformation response (duck-head-shaped curve) was observed in some specimens in their first cycle, but this response quickly disappeared in the following cycles due to degradation. Plump hysteretic responses, indicating good energy dissipation capacities (which will be discussed later in detail), were generally observed for the washers tested at room temperature (23 °C) and 10 °C, although the shape of the curve could vary with different specimens even under the same testing condition (e.g. SMA1-a and SMA1-b). This was probably due to the slight difference in the geometric dimensions of the specimens (note that the manufacturing tolerance was 0.1 mm for this batch of washers). The minor dimension difference can also be confirmed through specimen SMA2-S, where two SMA Belleville washers were stacked in series. In the first cycle of this specimen, fluctuation was observed in the loading (ascending) branch of the curve, and this was due to the varied duck-head responses of the two non-identical washers. From the second cycle, however, the load-deformation shape became smooth, which indicates that the two washers were deformed synchronously. It is worth pointing out that a larger cone angle (θ = 30°) was employed for the washers tested by Speicher et al. [21], and due to significant 'snap-through' tendency of each individual washer, the washer groups stacked in series showed pronounced fluctuation of the hysteretic curve. This highlights the importance of appropriate geometric design of the washers for desired applications.

At low temperatures (i.e. 0 °C and -20 °C), superelastic effect could not be fully developed for specimens SMA1-T(0~23) and SMA1-T(-20~23), and significant residual deformation was therefore induced after the first cycle. The load at maximum deformation in the first cycle was less than 7 kN for both specimens and a continuous decrease of this value was experienced with subsequent load cycles. After 10 loading cycles at low temperatures, the specimens were reheated, followed by another 50 loading cycles at room temperature. It was observed that the residual deformation was recovered after reheating, and stable hysteretic responses were shown during the extra 50 cycles. The stable load-deformation curves can probably be attributed to the initial low temperature 'training' process. Moreover, it is of interest to find that these hysteretic responses (after reheating) could be more plump

and stable than those of the specimens directly loaded at room temperature. This phenomenon may shed light on the optimal training process for SMA Belleville washers (as well as other SMA components), but further investigations are required on this front.

On the other hand, when the temperature increased beyond room temperature (i.e. 40 °C and 60 °C), the load-deformation curves became 'narrower', and the load at ultimate deformation increased with increasing temperature. This is coherent with previous research findings for axially loaded SMA wires under various temperatures, where it was generally observed that increasing the temperature could increase the forward/reverse loading plateaus as well as the residual deformation [27-29]. The increased residual deformation was caused by some amount of plastic (permanent) deformation of the specimens under elevated temperatures, where the required forward transformation stress might have exceeded the true yield (plastic) stress of the material. Finally, for the stainless steel washer SS1, significant residual deformation, due to plastic/permanent strain, was induced immediately after the initial loading cycle. Negligible recovery of deformation, as expected, was exhibited during the unloading process, and afterwards the stainless steel washer had completely lost its energy dissipation and deformability. The distinct difference between the stainless steel and SMA washers clearly demonstrates the unique response of Belleville washers when endowed with superelastic property offered by SMA.

3.2 *Strength and stiffness*

The strength of the SMA washers can be presented using the peak load recorded for each cycle, as shown in Fig. 5(a). For specimens SMA1-T(0~23) and SMA1-T(-20~23), the results of the initial ten loading cycles at low temperatures (i.e. 0 °C and -20 °C, respectively) are not shown in the figure. The peak loads of the specimens varied between 10 kN and 26 kN, where the variation was mainly due to the different temperatures and stack combinations. The peak load of the SMA washers increased with increase in temperature. This is due to the increase of the forward transformation plateau. When two washers were stacked in parallel, i.e. specimen SMA2-P, the peak load was doubled. In general, the peak load was almost kept constant throughout the 50 loading cycles. For some specimens, e.g. SMA1-b, the peak load increased very slightly with increasing number of cycles, and this might be due to minor latent heat effect, which is a common phenomenon during the phase transformation process of SMA [30]. The latent heat effect can change the internal temperature of SMA if the loading rate is sufficiently large, where the induced heat is unable to be fully dissipated. For the current tests, the loading frequency was 0.02 HZ, which should be low enough to allow most of the latent heat to be dissipated, and therefore, the latent heat effect on the peak load of the test specimens is considered to be minor. It is worth mentioning that during actual earthquakes, a larger loading rate is expected, a case which may lead to more significant latent heat effect and thus can influence the hysteretic response of the SMA washers. This may be worthy of further investigations.

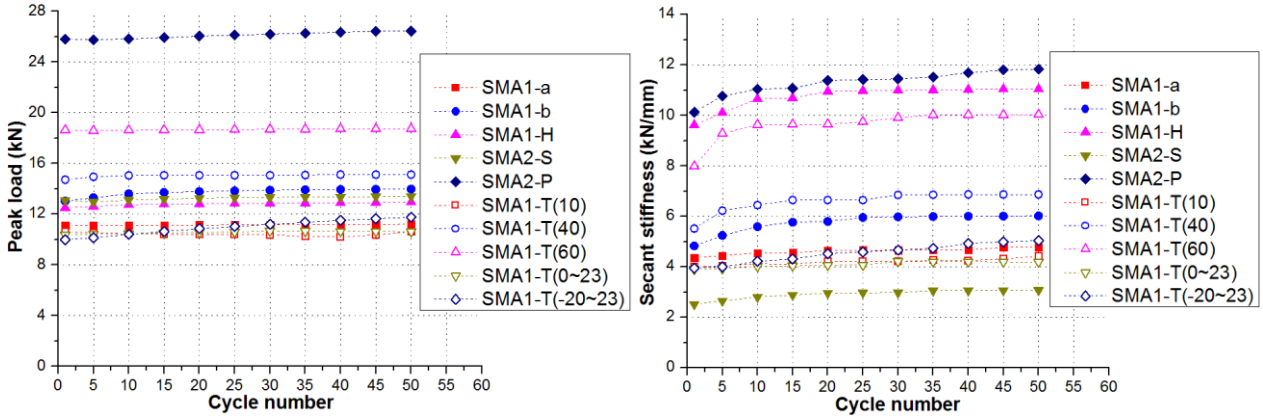

(a) (b)

Fig. 5 Strength and stiffness responses of SMA washer specimens

Fig. 5(b) shows the secant stiffness responses of the SMA washers. The secant stiffness for each cycle is calculated as the ratio of the peak load over the 'effective' deformation D_e, where D_e is obtained by deducting the accumulated residual deformation by the end of the previous cycle from the maximum compression (e.g. 2.7 mm). The secant stiffness of the specimens varied significantly (between 2.8 kN/mm and 12 kN/mm) with varying temperatures and stack combinations. The two washers stacked in parallel can lead to the secant stiffness four times of that for the washers stacked in series. This highlights the fact that desirable properties of SMA washer groups can be effectively achieved by simply adjusting the stack combinations. The secant stiffness was also influenced by the allowable maximum deformation. In addition, the secant stiffness of the washers increased with increasing number of cycles. This mainly results from the decreased D_e of each cycle with accumulated residual deformation.

3.3 Self-centring ability

Localized crystal slip during stress-induced martensitic transformation with possible defects on grain boundaries could cause residual deformations of SMA with increasing number of cycles [3]. As self-centring ability is one of the most important properties of the SMA washers, it is important that any SMA component for seismic control applications should have limited residual deformation during the service life, or the residual deformation could be controlled (i.e. stabilised) after a certain number of cycles. Fig. 6 shows the accumulated residual deformations of the SMA washers with increasing number of cycles. Again, for specimens SMA1-T(0~23) and SMA1-T(-20~23), only the results from the 50 loading cycles at room temperature are shown in the figure. For the individual SMA washers tested at 10 °C or 23 °C, the maximum accumulated residual deformation after 50 loading cycles was below 0.4 mm, corresponding to 14.8% of the maximum compressive deformation. In other words, more than 85% of the compressive deformation can be recovered after a significant number of repeated loading, which indicates good self-centring abilities of the SMA washers. It is also noted that

when two SMA washers were stacked in series (i.e. specimen SMA2-S), the total accumulated residual deformation, which was contributed by that induced by two washers, was almost doubled. With increasing temperatures, the residual deformation was also increased. The residual deformation could be accumulated up to 0.78 mm (29% of the maximum deformation) after 50 loading cycles when the temperature attained 60 °C.

It was clearly shown that for all the specimens, the residual deformation was quickly developed during initial loading cycles (e.g. during the first ten cycles). Subsequently the accumulation of the residual deformation started to slow down evidently. For most washers, more than 60% of the total residual deformation was developed within the first ten cycles. This implies that for practical use of SMA washers, a 'pre-training' process with ten fully compressed loading cycles may effectively stabilise the residual deformation of the considered SMA washers when subjected to further loading cycles. It is worth mentioning that for SMA washers with other geometric configurations (e.g. different cone angles), the necessary pre-training cycles to stabilise residual deformation may be different, and further studies are required towards optimisation of the pre-training schemes for SMA washers. Furthermore, some previous studies on SMA bolts [15] showed that applying preload can effectively reduce the residual deformations during their service life, and this finding also applies to SMA washers. For structural engineering applications, e.g. washers for self-centring connections [17] or dampers, a preload (i.e. pre-compression) can be applied, and in this case, pre-training may be unnecessary from a self-centring point of view. Based on the test results shown in Fig. 6, a preload leading to at least 15% of the flattened deformation may eliminate the residual deformation of the considered SMA washers under ambient conditions, and the level of preload may need to be increased with increasing working temperature.

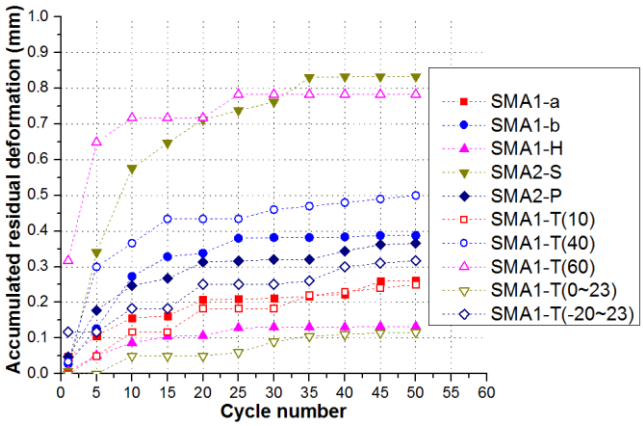

Fig. 6 Residual deformation responses of specimens

3.4 *Energy dissipation*

The cyclic response of the SMA washers also exhibits their potential for energy dissipation applications (or at least for supplementary energy dissipation applications) such as damping and base

isolation systems. The energy dissipation per cycle, which is obtained by the loop area enclosed by the load-deformation hysteretic curve, is shown in Fig. 7(a). It was generally observed that the energy dissipation tended to decrease with increasing number of cycles, which was due to the TIF effect of SMA. At the first cycle, a higher level of energy dissipation was exhibited when the working temperature was high. This was due to the increase of the forward transformation plateau (recalling the martensite/austenite slopes shown in Fig. 4) which tended to increase the area enclosed by the hysteretic loop, thus increasing the absolute energy dissipation. However, the energy dissipation per cycle decreased quickly in the subsequent loading cycles due to the significantly 'narrowed' hysteretic shapes, as can be typically seen in the result for specimen SMA1-T(60). On the other hand, for the individual SMA washers tested at room temperature or 10 °C, the energy dissipation per cycle was more stable under repeated loading cycles. When the SMA washer was loaded with half of the maximum deformation, i.e. specimen SMA1-H, the energy dissipation per cycle was significantly decreased. It was observed that upon stabilisation (e.g. after ten loading cycles), the energy dissipation per cycle of specimen SMA1-H was only about 30% of that for the fully compressed specimens. This implies that an effective consumption of the allowable deformation of SMA washers/washer groups is preferred for effective exploitation of their energy dissipation potential, and therefore, it is recommended that the arrangement of SMA washers (maximum deformation) may match the target deformation (e.g. drift) of the overall structures, such that the allowable deformation can be effectively utilised. Furthermore, the variable stack combinations of the SMA washers can further diversify their energy dissipation properties. When stacked in parallel (e.g. specimen SMA2-P), the energy dissipation was almost doubled with the same maximum deformation. However, when stacked in series (e.g. specimen SMA2-S), doubled energy dissipation was also obtained but with a corresponding doubled maximum deformation.

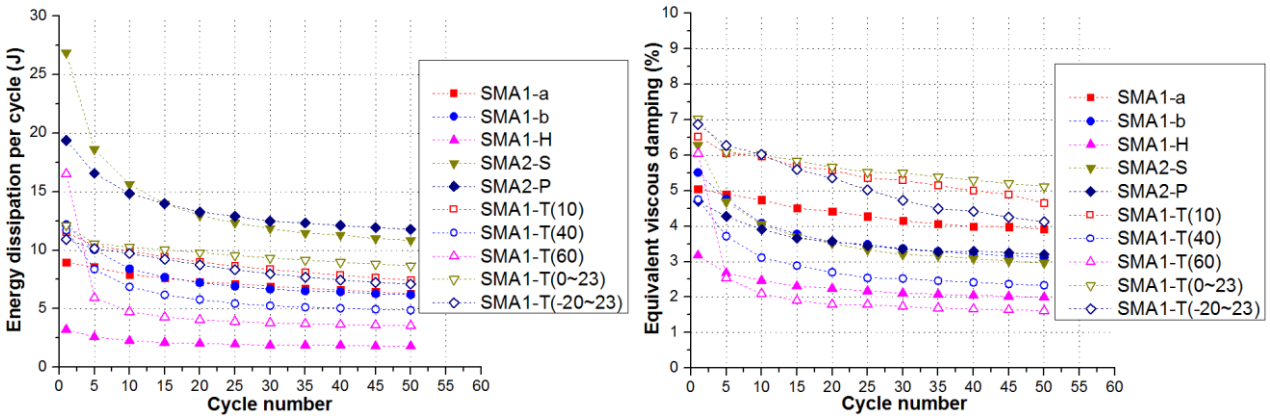

(a) (b)

Fig. 7 Energy dissipation responses of specimens

The energy dissipation capability of the SMA washers can be alternatively presented by a mathematically convenient coefficient, namely, equivalent viscous damping (EVD) ξ_{eq}, as defined by:

$$\xi_{eq} = \frac{W_D}{4\pi W_E} \quad (1)$$

where W_D is the energy loss per cycle as shown in Fig. 7(a), and W_E is the strain energy stored in a linear system that has the same maximum load and deformation [28]. EVD is normally related to the shape of the hysteretic loop, but is not directly dependent on the actual value of the force or displacement; therefore, EVD can be considered as a 'size-independent' measurement of energy-dissipating ability. It was observed that for the tested specimens, an EVD of up to 7% could be achieved for the first loading cycle. Again, the EVD tends to decrease with increasing number of cycles due to the decrease in the amount of dissipated energy per cycle. Specimens SMA1-T(10), SMA1-T(0~23), and SMA1-T(-20~23) exhibited relatively high EVDs among all the specimens, and this echoes the plump shapes of the load-deformation responses of these specimens shown in Fig. 3. After 50 loading cycles, the EVDs of all the SMA washers ranged between 1.7% and 5.1%.

Furthermore, the EVDs of the SMA washers can be compared with those of uniaxially loaded SMA wires or bars which are considered as the most effective form of SMA components. Previous studies [31] showed that the EVDs of SMA wires and bars tested at ambient temperature generally ranged between 2% and 7% when subjected to a reasonable strain value (between 3% and 6%). It should be noted that those SMA wires and bars were tested with only a few cycles (normally less than 10 cycles), so it is expected that their EVDs would be further reduced if subjected to further loading cycles. For the SMA washers tested at room temperature in this study, the EVDs at the 10^{th} cycle ranged between 4% and 6%, which were comparable with those of the uniaxially loaded SMA wires or bars. This indicates that from the EVD point of view, the SMA washers with the current geometric configuration can lead to similar energy dissipation responses as uniaxial SMA components, and therefore the washers can be considered as an alternative solution to SMA wires or bars, especially when compressive loading resistance is desirable.

4. Numerical study and further discussions

A numerical study was conducted to further discuss the behaviour of the SMA Belleville washers under compression. In particular, the numerical models can reveal the stress/strain conditions which are difficult to be fully monitored through the tests. The numerical study may also help explain some test phenomena which have been previously discussed in this article. The general nonlinear Finite Element (FE) programme ABAQUS [32] was employed for the numerical study. Efficient 8-node linear brick elements, namely, C3D8 in ABAQUS nomenclature, were considered for the SMA washers. The mesh size was approximately 1 mm × 1 mm, leading to four layers of elements over the thickness of the washer. A rigid cover plate was attached to the top of the washer model, and a 'hard contact' was defined between the cover plate and the washer to simulate the actual contact condition between the top cylinder and the specimen. The bottom of the washer model was supported vertically

but were free to move laterally to allow expansion of the washer under compression. The compressive load was applied on a reference point located at the centroid of the cover plate. The analysis was performed using the general standard static solver. For the material model of SMA, a user-defined thermal-mechanical model using the Auricchio's approach [33] was employed to simulate the superelastic effect of SMA at different temperatures. The key material parameters for superelatic SMA in ABAQUS include critical transformation stresses (σ_{Ms}, σ_{Mf}, σ_{As}, and σ_{Af}), Young's Moduli (E_A and E_M), maximum transformation strain ε_L, martensite/austenite slopes (C_M and C_A), Poisson's Ratios (ν_A and ν_M), and thermal expansion coefficient of austenite (α_A). The adopted values of these parameters are presented in Table 2. In addition, the basic definitions of the parameters have been illustrated in Fig. 4 for ease of understanding.

Table 2 Material properties of SMA used in ABAQUS

Material properties	Value
Forward transformation stress σ_{Ms}	430 MPa
Forward transformation stress σ_{Mf}	480 MPa
Reverse transformation stress σ_{As}	250 MPa
Reverse transformation stress σ_{Af}	150 MPa
Young's Modulus (Austenite) E_A	60 GPa
Young's Modulus (Martensite) E_M	40 GPa
Martensite slope C_M	6.7 MPa/°C
Austenite slope C_A	8.3 MPa/°C
Maximum transformation strain ε_L	5%
Poisson's Ratio (Austenite) ν_A	0.33
Poisson's Ratio (Martensite) ν_M	0.33
Coefficient of thermal expansion α_A	1.13×10^{-5}/°C

It should be noted that the material properties given in Table 2 are based on a series of tensile coupon tests [16] on large size SMA bars (shank diameter from 10 mm to 20 mm) ordered from the same material supplier with the same nominal chemical composition as the current SMA Belleville washers. However, as observed in the tensile coupon test results [16], the stress-strain response changed with different loading cycles (i.e. due to degradation effect), which is difficult to reflect via the current constitutive model. Even at the same strain level, deviations of material properties were observed for different coupons, probably due to the size effect. This further complicates the determination of the key material parameters for the current study. Therefore, considering the uncertainty of the basic material parameters, a representative material model, which led to a reasonable match in terms of the load-deformation response of the washer at room temperature (23 °C), was considered. The representative material model adopted six basic parameters σ_{Ms}, σ_{Mf}, σ_{As},σ_{Af}, E_A and E_M (based on the coupon test results) to reflect the superelastic effect of SMA at room temperature. Two other parameters, namely, martensite/austenite slopes (C_M and C_A) were required to reflect the change of forward/reverse plateaus with the change of temperature. The values of C_M and

C_A given in Table 2 are based on the typical test results reported in [3]. For the remaining material parameters, e.g. ε_L, v_A, v_M, and α_A, standard values [3] were employed.

As the current Auricchio's model is not capable of modelling the effects of stress degradation and residual deformation due to TIF, the initial cycle of each load-deformation curve was used for validation purposes. Fig. 8 shows the comparisons of the load-deformation response between the selected test results and FE predictions. It should be noted that for the two single washers tested at room temperature (i.e. duplicate specimens SMA1-a and SMA1-b), the average tested load-deformation response was used. Good agreements were observed for the washers at temperatures ranging from 10 °C to 40 °C, but more obvious discrepancies were observed for the case of 60 °C (especially in the unloading curve), where the significant residual deformation observed in the test is not reflected in the FE prediction. Although TIF was not considered in the numerical study, the stress conditions revealed by the FE models may help explain the high level of residual deformation observed in the washer at high temperatures.

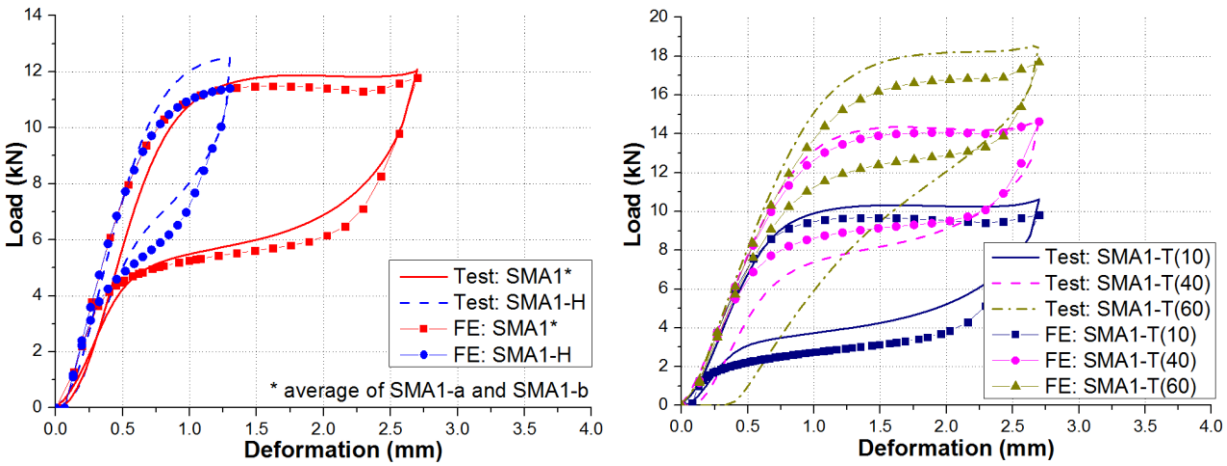

Fig. 8 Comparison of load-deformation response – test results vs. FE predictions

Fig. 9 shows the stress states of the washer at varying deformation states at room temperature (23 °C). Non-uniform stress distributions are generally observed, where the maximum tensile stress occurs near the lower part of the outer ring edge (location 3) whilst the maximum compressive stress is developed near the upper part of the inner ring edge (location 1). The area crossing the 'diagonal zone' linking locations 2 and 4 remains under low stress levels throughout the loading cycle. At the maximum displacement (2.7 mm), the maximum tensile and compressive stresses are approximately 500 MPa and 530 MPa, respectively, which indicates that a full forward transformation is completed at these locations (noting that σ_{Mf} = 480 MPa). Upon unloading, the stress level decreases rapidly, and when the loading cycle is completed, no residual stress is developed. Fig. 10 shows the influence of temperature on the stress state of the washer at the maximum displacement. It can be seen that the stress level increases remarkably with increasing temperature. At 60 °C, the maximum stress can be

greater than 800 MPa, which is twice of that observed for the case of 10 °C. The increase in the stress level with increasing temperature is due to the austenite/martensite slopes (C_A and C_M) which are inherent thermal-mechanical properties of SMA. The high level of stress can lead to more pronounced TIF, leading to increased residual deformation and more significant stress degradation, as observed from the test results. As confirmed by the FE results, the evident residual deformation of specimen SMA1-T(60) can be due to the fact that parts of the specimen experienced stress levels exceeding the true yield (plastic) stress at 60 °C.

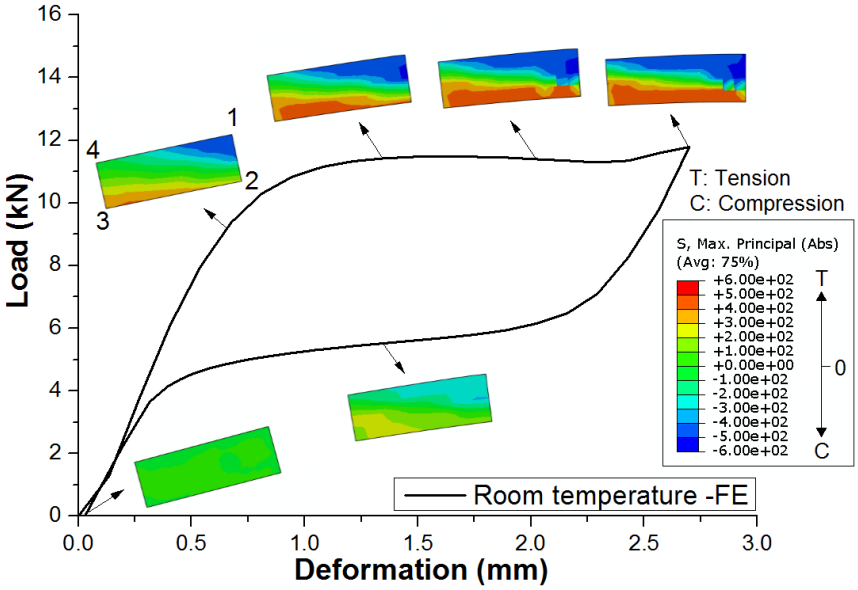

Fig. 9 Stress conditions at different deformation stages

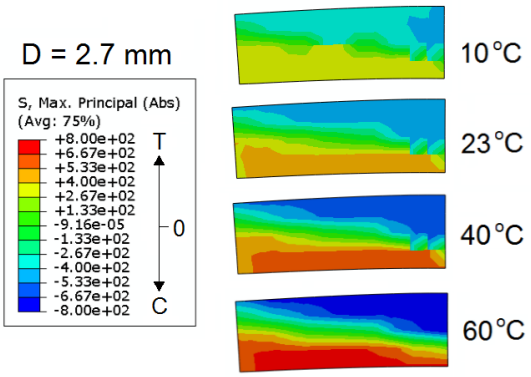

Fig. 10 Influence of temperature on stress conditions

In general, some test phenomena are well explained by the numerical models, which are also shown to have potential for initial design of SMA Belleville washers, provided that the basic material properties can be provided by the material manufacturer. The validated FE model may also be used for further parametric studies (e.g. varying geometric dimensions, maximum deformations, and

temperatures) towards optimal design of such washers for the purpose of resisting seismic actions, but this is not within the scope of the current study.

5. Phenomenological modelling

While the basic properties of SMA components could be modelled from the afore-mentioned FE study, some key phenomena, including the degradation effect, could not be sufficiently captured. To address this, a constitutive model was developed in the MATLAB environment [34] to simulate the hysteretic responses, taking account of the degradation effects under varied temperatures. The model was developed over the force-displacement domain with a bidirectional response. Based on the main findings from the current study, the constitutive model of a typical damping device incorporating a group of SMA Belleville washers is schematically illustrated in Fig. 11. According to the test results, two parameters, namely, forward transformation start force F_{ms}, and residual displacement Δ_{res}, varied obviously with increasing loading cycles, whereas other parameters almost remained unchanged. Therefore, these two parameters were considered as loading history related variables in the constitutive model, and other key parameters, including K_a, K_m, F_{max}, F_{as}, F_{af}, and Δ_{max} were considered as constants and could be obtained via the available test data with an idealisation process as typically shown in Fig. 11. The proposed hysteresis rules are described as follows.

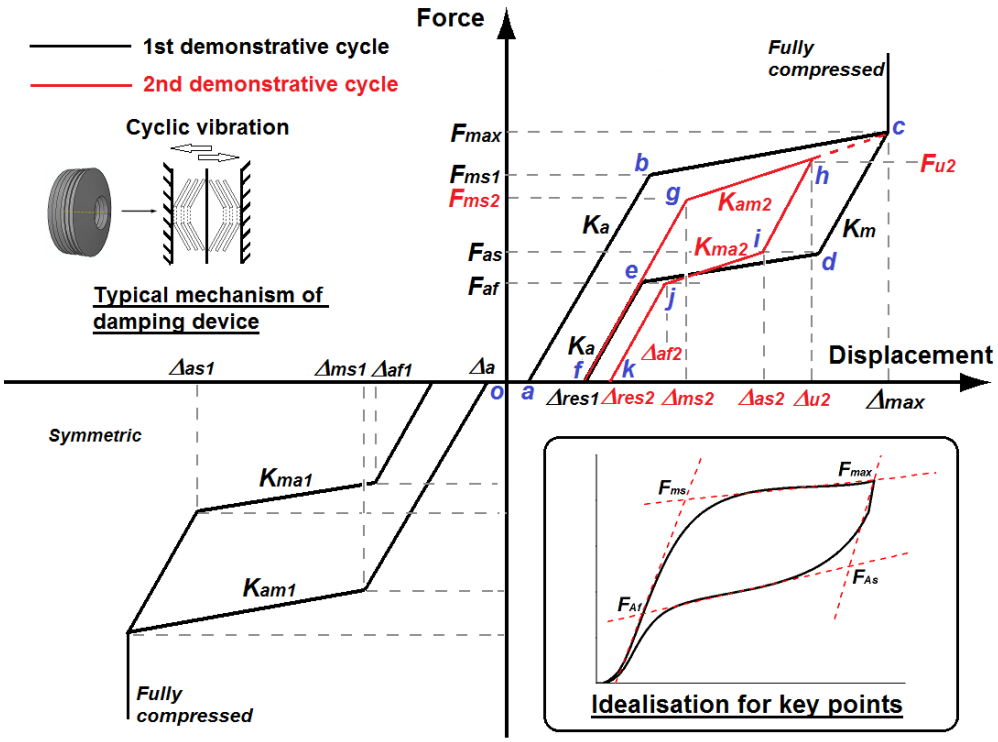

Fig. 11 Demonstration of hysteresis rule for SMA Belleville washers

- *Initial zero-stiffness path* (*o-a)*: this is a zero-stiffness stage which is observed in the test results. The *o-a* path is mainly caused by the non-perfect initial contacting condition between the loading

head and the washer, and may be ignored as the corresponding displacement is small. However, for general applicability, this stage is still included in the constitutive model.

- *Initial loading path* (*a*-*b*): during this stage, the washers remain in the austenite state, and linear response is exhibited with an initial stiffness K_a. The force-displacement (F-Δ) relationship follows the equation, $F = K_a(\Delta-\Delta_a)$. The stage ends when the forward transformation start force F_{ms1} is achieved.
- *Forward transformation path* (*b*-*c*): this stage starts with the occurrence of forward transformation of the SMA material. The stiffness K_{am1} could be obtained from test results, and the value may be affected by both material and geometric nonlinearities. The stage ends when the washers are fully compressed, after which the stiffness becomes infinite. The relationship, $F = F_{ms1} + K_{am1}(\Delta-\Delta_{ms1})$, is followed, and in this cycle, $K_{am1} = (F_{max}-F_{ms1})/(\Delta_{max}-\Delta_{ms1})$.
- *Martensite unloading path* (*c*-*d*): The washers are unloaded linearly with an unloading stiffness K_m. This stage ends upon the initiation of reverse transformation, and the F-Δ relationship follows $F = F_{max} + K_m(\Delta-\Delta_{max})$. For simplicity of the model, and according to the test observation, K_m may be taken to be equal to K_a.
- *Reverse transformation path* (*d*-*e*): this stage starts with the occurrence of reverse transformation of the SMA material with stiffness K_{ma1}. Due to the degradation effect, the reverse line intersects with an offset line which is parallel to the initial loading line, but is horizontally shifted by the accumulated residual displacement induced due to the previous loading history. During this stage, a F-Δ relationship, $F = F_{as} + K_{ma1}(\Delta-\Delta_{as1})$, is followed, and the stiffness $K_{ma1} = (F_{as}-F_{af})/(\Delta_{as1}-\Delta_{af1})$ is obtained, where $\Delta_{af1} = \Delta_{res1} + F_{af}/K_a$. The determination of the accumulated residual displacement is elaborated later.
- *Austenite unloading path* (*e*-*f*): following the completion of the reverse transformation process, the washers further unloads with stiffness K_a, i.e. $F = K_a(\Delta-\Delta_{res1})$, and the resulting residual displacement after complete unloading is Δ_{res1}.
- *Gap path* (*between f and o via a*, and possibly travel to opposite directions): this is a zero-stiffness range reflecting the gap induced in the device incorporating SMA Belleville washer groups.
- *Reloading path* (*f*-*g*): after gap closure, the load resistance is regained, and the loading path now starts at point *f* with the stiffness K_a, and in this stage $F = K_a(\Delta-\Delta_{res1})$. Due to the degradation effect, this stage ends when the degraded forward transformation start force F_{ms2} is achieved, where the corresponding displacement is $\Delta_{ms2} = \Delta_{res1}+F_{ms2}/K_a$. The decrease of F_{ms} is also related to the previous loading history, as discussed in detail later.

- *Second forward transformation path* (*g*-*h*): forward transformation is induced again after F_{ms2} is reached, and the updated stiffness is $K_{am2} = (F_{max}-F_{ms2})/(\Delta_{max}-\Delta_{ms2})$. The relationship of $F = F_{ms2} + K_{am2}(\Delta-\Delta_{ms2})$ is followed.
- *Second unloading path* (*h*-*i*): with the same unloading stiffness as that considered for path *c*-*d*, the load decreases linearly until F_{as}. This can be confirmed through comparing the test result of SMA1-a (or SMA1-b) with that of SMA1-H, where a similar level of F_{as} was observed although the maximum compressed deformation is different.
- *Second reverse transformation path* (*i*-*j*): again, due to the degradation effect, the reverse line intersects with an offset line which is further shifted according to the new accumulated residual displacement Δ_{res2}. During this stage, the F-Δ relationship follows $F = F_{as} + K_{ma2}(\Delta-\Delta_{as2})$, and the stiffness $K_{ma2} = (F_{as}-F_{af})/(\Delta_{as2}-\Delta_{af2})$, where $\Delta_{af2} = \Delta_{res2} + F_{af}/K_a$.

After path *i*-*j*, the subsequent unloading (*j*-*k*) and reloading responses are similar to those discussed above. For the proposed model, the varying parameters F_{ms} and Δ_{res} were considered with an indicator named as 'accumulated transformation displacement history' Δ_{total}, which is the total forward transformation displacements accumulated from all the previous loading history. Employing this strategy, the conditions of F_{ms} and Δ_{res} could be correlated to random loading histories. Based on the current test data, the accumulated displacement Δ_{total} versus F_{ms} or Δ_{res} responses for the washers under three different temperatures, i.e. SMA1-a, SMA1-T(40), SMA1-T(60) are shown in Fig. 12. The trends could be presented via a unified exponential equation, as expressed by:

$$f(x) = a\exp(-bx) + c \tag{2}$$

The coefficients *a*, *b* and *c* in Eq. (2) were obtained using the MATLAB curve fitting tool, and they are listed in Table 3. Comparisons between the measured test data and the fitted curves are shown in Fig. 12, where it can be seen that the exponential form well captures the cycle dependent effect at various temperatures.

Table 3 Coefficients for cycle dependent curve fitting

Specimen	Item	a	b	c
SMA1-a	F_{ms}	2.913	0.021	7.320
	Δ_{res}	-0.194	0.043	0.350
SMA1-T(40)	F_{ms}	4.354	0.065	9.610
	Δ_{res}	-0.460	0.156	0.514
SMA1-T(60)	F_{ms}	5.700	0.201	11.870
	Δ_{res}	-0.748	0.391	0.827

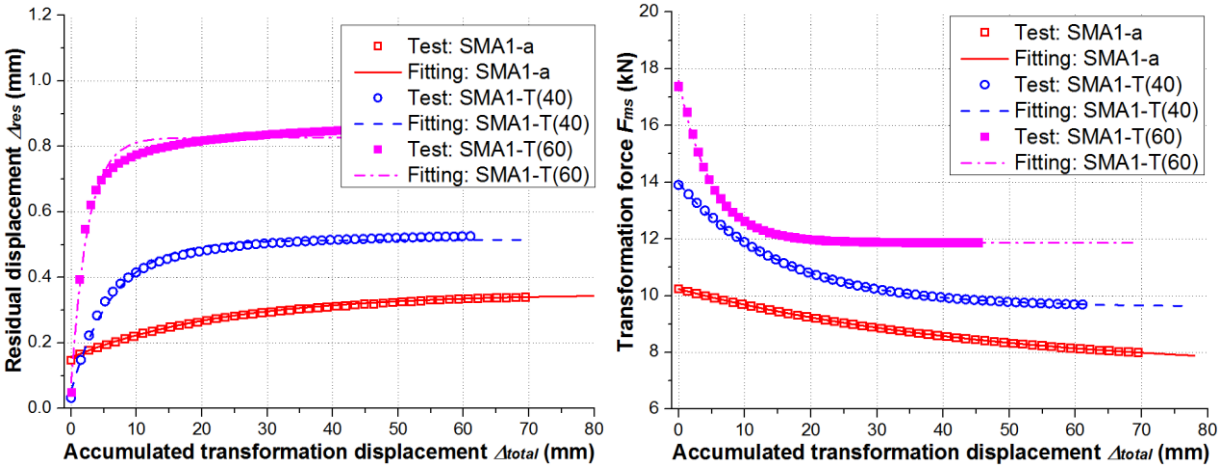

Fig. 12 Degradations of forward transformation force and residual displacement

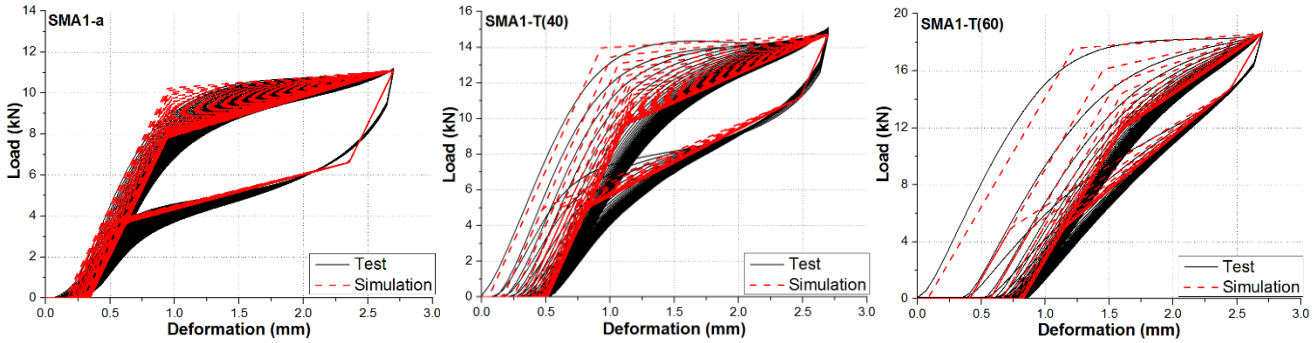

Fig. 13 Comparisons between test and simulation results

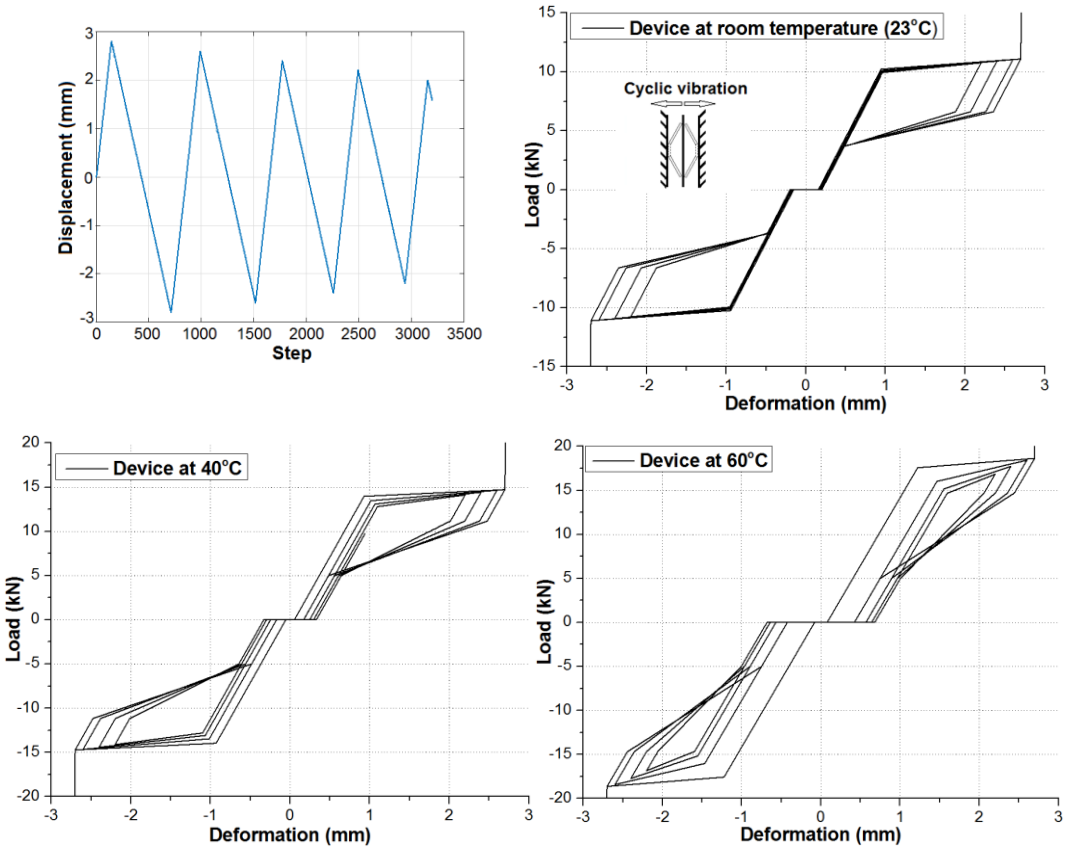

Fig. 14 Typical responses of SMA device subjected to random displacement history

Employing the above-mentioned modelling strategy, the simulation results are compared with the test results as shown in Fig. 13. Good agreements in terms of the load-deformation response were observed between the test and simulation results, and the degradation effects at different temperatures are sufficiently reflected by the proposed constitutive model. In order to further demonstrate the application of the model, the general cyclic load-deformation responses of a typical seismic resisting device incorporating the tested SMA Belleville washers are shown in Fig. 14. For illustrative purposes, the device is comprised of two washers, each responsible for the corresponding load from one direction, as schematically sketched in the figure. It should be noted that the model could be easily modified to consider other washer combination patterns. A random bidirectional loading history was applied onto the device, and three working temperatures, namely, 23 °C, 40 °C, and 60 °C, were considered. The simulation results show that the model is capable of capturing the key hysteretic properties of the device. In addition, the model has good numerical robustness, making it an effective and reliable tool for simulating SMA devices under various working conditions. If other SMA Belleville washer type are considered in future, practical engineers could still use the current modelling framework to establish desirable models if the relevant test data are available.

6. Summary and conclusions

A comprehensive study on cyclic mechanical properties of superelastic SMA Belleville washers/springs was conducted, highlighting a great potential of using such components for seismic resisting devices. The test results showed satisfactory self-centring ability, repeatability, and energy dissipation capacities of these washers at 10 °C and 23 °C, and a good flexibility in load resistance and allowable deformation could be realised through changing the stack combination, i.e. in series or in parallel. Depending on the temperature and stack combination, the peak loads of the specimens varied between 10 kN and 26 kN, and a maximum equivalent viscous damping of 7% was observed. For the individual SMA washers tested at 10 °C or 23 °C, the maximum accumulated residual deformation after 50 loading cycles was below 0.4 mm, corresponding to a recovery rate of more than 85%. Although slight degradations of the hysteretic responses accompanied by residual deformations were induced in the first few cycles, the hysteretic loop was quickly stabilised. No such performance was observed for the stainless steel washer (which was tested for comparison purposes), where significant residual deformation was induced immediately after the first loading cycle.

At low temperatures (i.e. 0 °C and -20 °C), superelastic effect could not be fully developed due to the gradual loss of superelasticity. Nevertheless, the induced residual deformation was almost fully recovered after reheating, and subsequently good hysteretic responses were shown when subjected to 50 more cycles at room temperature. On the other hand, when the temperature increased beyond room temperature (i.e. 40 °C and 60 °C), the load at ultimate deformation increased, but more residual deformation was induced due to a certain amount of plastic deformation of the specimens under

elevated temperatures. A numerical study using the general FE programme ABAQUS was adopted to further discuss this mechanism, where the stress/strain conditions, which are difficult to be fully monitored through the tests, were revealed at varying working temperatures. Following the experimental and numerical study, a phenomenological model, accounting for the degradation effects under varied temperatures, was developed to enable effective and accurate simulation of seismic devices incorporating SMA Belleville washers. The constitutive model, which was programmed in MATLAB environment, was shown to have good numerical robustness, and through comparisons with the test data, good agreements were observed in terms of the hysteretic responses.

Acknowledgements

The work presented in this paper is supported by the National Natural Science Foundation of China (NSFC) with Grant No. 51408437. The support from the 'Program for Young Excellent Talents in Tongji University' is also gratefully acknowledged.

References

[1] Mani G, Feldman MD, Patel D, Agrawal M. Coronary stents: A materials perspective. Biomaterials 2007; 28(9):1689-710.

[2] Chandra R. Active shape control of composite blades using shape memory actuation. Smart Materials & Structures 2001; 10(5):1018-1024.

[3] Lagoudas DC. Shape memory alloys: modeling and engineering applications. Springer; USA, 2008.

[4] Song G, Ma N, Li HN. Applications of shape memory alloys in civil structures. Engineering Structures 2006; 28(9):1266-1274.

[5] Dezfuli FH, Alam MS. Shape memory alloy wire-based smart natural rubber bearing. Smart Materials & Structures 2013; 22(4):361-373.

[6] Ozbulut OE, Hurlebaus S. Seismic assessment of bridge structures isolated by a shape memory alloy/rubber-based isolation system. Smart Materials & Structures 2010; 20(1):15003-15014.

[7] Zhang Y, Zhu S. A shape memory alloy-based reusable hysteretic damper for seismic hazard mitigation. Smart Materials & Structures 2007; 16(5):1603-1613.

[8] Parulekar YM, Ravi Kiran A, Reddy GR, Singh RK, Vaze KK. Shake table tests and analytical simulations of a steel structure with shape memory alloy dampers. Smart Materials & Structures 2014; 23(12):125002-125013.

[9] Massah SR, Dorvar H. Design and analysis of eccentrically braced steel frames with vertical links using shape memory alloys. Smart Materials & Structures 2014; 23(11).

[10] McCormick J, DesRoches R, Fugazza D, Auricchio F. Seismic Assessment of Concentrically Braced Steel Frames with Shape Memory Alloy Braces. Journal of Structural Engineering 2007; 133(6):862-870.

[11] Yang CSW, Desroches R, Leon RT. Design and analysis of braced frames with shape memory alloy and energy-absorbing hybrid devices. Engineering Structures 2010; 32(2):498-507.

[12] Beltran JF, Cruz C, Herrera R, Moroni O. Shape memory alloy CuAlBe strands subjected to cyclic axial loads. Engineering Structures 2011; 33(10):2910-2918.

[13] Reedlunn B, Daly S, Shaw J. Superelastic shape memory alloy cables: Part I – Isothermal tension experiments. International Journal of Solids & Structures 2013; 50(20-21):3009-3026.

[14] Speicher MS, Desroches R, Leon RT. Experimental results of a NiTi shape memory alloy (SMA)-based recentering beam-column connection. Engineering Structures 2011; 33(9):2448-2457.

[15] Fang C, Yam MCH, Lam ACC, Xie LK. Cyclic performance of extended end-plate connections equipped with shape memory alloy bolts. Journal of Constructional Steel Research 2014; 94(94):122-136.

[16] Fang C, Yam MCH, Ma HW, Chung KF. Tests on superelastic Ni–Ti SMA bars under cyclic tension and direct-shear: towards practical recentring connections. Materials & Structures 2013; 48(4):1013-1030.

[17] Yam MCH, Fang C, Lam ACC, Zhang YY. Numerical study and practical design of beam-to-column connections with shape memory alloys. Journal of Constructional Steel Research 2015; 104:177-192.

[18] Desroches R, Delemont M. Seismic retrofit of simply supported bridges using shape memory alloys. Engineering Structures 2002; 24(3):325-332.

[19] Fromm E, Kleiner W. Handbook for Disc Springs, Schnorr Corporation, Hela Werbung, Hellbronn, 2003.

[20] Labrecque C, Braunovic M, Terriault P, Trochu F, Schetky M. Experimental and theoretical evaluation of the behavior of a shape memory alloy Belleville washer under different operating conditions. Proceedings of the annual Holm conference on electrical contacts, IEEE, Chicago, 1996.

[21] Speicher M, Hodgson DE, DesRoches R, Leon RT. Shape Memory Alloy Tension/Compression Device for Seismic Retrofit of Buildings. Journal of Materials Engineering & Performance 2009; 18(5-6):746-753.

[22] Fang C, Vemury C, Yam MCH. A numerical study of cyclic behaviour of NiTi shape memory alloy belleville washers. Proceedings of the International Conference on Advances in Civil, Structural and Mechanical Engineering, Birmingham, 2014.

[23] Maletta C, Filice L, Furgiuele F. NiTi Belleville washers: Design, manufacturing and testing. Journal of Intelligent Material Systems & Structures 2013; 24(6):695-703.

[24] Sgambitterra E, Maletta C, Furgiuele F. Modeling and simulation of the thermo-mechanical response of NiTi-based Belleville springs. Remote Sensing of Environment 2014; 113(2):445-457.

[25] Fang C, Yam MCH, Lam ACC, Zhang YY. Feasibility study of shape memory alloy ring spring systems for self-centring seismic resisting devices. Smart Materials & Structures 2015; 24(7): 075024.

[26] Gao N, Jeon JS, Hodgson DE, DesRoches R. An innovative seismic bracing system based on a superelastic shape memory alloy ring. Smart Materials & Structures 2016; 25:055030.

[27] Tobushi H, Shimeno Y, Hachisuka T, Tanaka K. Influence of strain rate on superelastic properties of TiNi shape memory alloy. Mechanics of Materials 1998; 30(2):141-150.

[28] Dolce M, Cardone D. Mechanical behaviour of shape memory alloys for seismic applications 2. Austenite NiTi wires subjected to tension. International Journal of Mechanical Sciences 2001; 43(11):2657-2677.

[29] Churchill CB, Shaw JA, Iadicola MA. Tips and tricks for characterizing shape memory alloy wire: part 2—fundamental isothermal responses. Experimental Techniques 2009; 33(1):51-62.

[30] Tabesh M, Lester B, Hartl D, Lagoudas D. Influence of the latent heat of transformation and thermomechanical coupling on the performance of shape memory alloy actuators. ASME 2012 Conference on Smart Materials, Adaptive Structures and Intelligent Systems, Aerospace Division, Aerospace Division 2012; 8(3):237-248.

[31] DesRoches R, McCormick J, Delemont MA. Cyclical properties of superelastic shape memory alloys. Journal of Structural Engineering 2004; 130(1):38-46.

[32] ABAQUS. Analysis User's manual, v6.12, Dassault Systems Simulia Corp., Providence, USA, 2012.

[33] Auricchio F, Taylor RL, Lubliner J. Shape-memory alloys: macromodelling and numerical simulations of the superelastic behaviour. Computer Methods in Applied Mechanics and Engineering 1997; 146:281–312.

[34] MATLAB, version 7.10.0, The MathWorks Inc.; 2010.